

# The principle underlying antiaromaticity

Raphael J. F. Berger<sup>1\*</sup> and Alexandre Viel<sup>2</sup>

<sup>1</sup>Department for Chemistry and Physics of Materials, University of Salzburg,  
Jakob-Haringerstr 2a, A-5020 Salzburg, AUSTRIA

<sup>2</sup>8 Sente de la haie Saint-Marc, 78480 Verneuil sur Seine, FRANCE

\*To whom correspondence should be addressed; E-mail: raphael.berger@sbg.ac.at.

## Abstract

Aromaticity is one of the most widely used chemical concepts. Current definitions are purely phenomenological and relate symmetry, reactive stability and the occurrence of molecular diamagnetic response currents. The antithetical concept of antiaromaticity provides a connection between the contrary properties of structural instability or distortion out of higher symmetry, a small HOMO—LUMO gap, and paramagnetic response currents. We reveal the principle that is underlying antiaromaticity in showing an intimate and strict symmetry induced relation between these properties. This principle can be proven and is formulated like: *First order (and related) Jahn-Teller distorted molecules out of non-isometric point groups are prone to paramagnetic current susceptibility parallel to the main axis of symmetry.* We show by the exemplary cases of cyclobutadiene, cyclooctatetraene, pentalene and manganese trifluoride how this principle works and discuss this new perspective on antiaromaticity.

## 1 Introduction

Aromaticity is one of the most widely used chemical concepts. It aims at an abstraction of experimentally observed properties in a class of chemical compounds, that are typically high structural or energetic stability, proneness to specific chemical reactions and susceptibility to induced diamagnetic currents when at the same time a theoretical description or also experimental evidence suggests a specific type of electronic structure, often encountered in the form of electron count rules, orbital occupation patterns or electronic resonance<sup>1</sup>. A good overview about the state of research including references to a selection of current reviews is given in the introduction of<sup>2</sup>. While the connection of some of these properties seems obvious, no concise

connection between all in full generality could ever be established. Here we analyze the antithetical concept of *antiaromaticity* which was originally introduced by Breslow<sup>3</sup> and find an intimate symmetry relation between its defining properties which so far seems to have escaped the general attention. Along the lines of the definition of antiaromaticity from the Gold Book of the International Union of Pure and Applied Chemistry (IUPAC)<sup>4,5</sup> these are the three properties a) "... prone to reactions causing changes in their structural type, and display tendency to alternation of bond lengths and fluxional behavior ...", b) "... a small energy gap between their highest occupied and lowest unoccupied molecular orbitals ..." and c) "... an external magnetic field induces a paramagnetic electron current." A full quote of this definition is given in the SI. To show how these properties are related we use the following arguments

- Paramagnetic molecular response is determined by virtual excitations of rotational symmetry, where the axis of rotation is parallel to the magnetic field.
- Ground state—excited state (or HOMO—LUMO) symmetries that give rise to virtual excitations of rotational symmetry are arising from certain Jahn-Teller (JT) distortions out of specific molecular point group symmetries.
- These certain JT distortions are first order JT distortions (or closely related ones, which we later call *primoid* second order JT distortions) and which happen out of point group symmetries that are non-isometric. That is from one of the point groups  $C_n$ ,  $C_{nv}$ ,  $C_{nh}$ ,  $D_n$ ,  $D_{nh}$  for  $n > 2$ , and  $D_{nd}$  and  $S_{2n}$  for  $n > 1$ .

A consequence of these arguments and our main result is

*First order and primoid second order JT distorted molecules out of non-isometric point groups are prone to paramagnetic current susceptibility parallel to the main axis of symmetry.*

We then advocate the view that this is the symmetry principle underlying antiaromaticity. After derivation of these results we discuss some exemplary cases and important implications of this new perspective on antiaromaticity for past and future research and a possible extension to the concept of aromaticity.

The occurrence of paramagnetic response currents is one of the three central defining properties of antiaromatic molecules. We start the discussion with a derivation of a symmetry based "selection rule" for virtual excitations determining paramagnetic response currents.

## 2 Paramagnetic response currents

When a molecule is exposed to a magnetic field  $\mathbf{B}$ , that is in the simplest case static, homogeneous and weak, which we assume throughout this work, it interacts to first order via the total electronic angular momentum and total spin which correspond to permanent molecular magnetic moments. In case the expectation values of both are identical zero, *i.e.* closed shell singlet

molecules, it only interacts to second order via its molecular magnetisability which is for bulk mater also called magnetic susceptibility. In the quasi-classic Bohr model of electrons circling around the nucleus such a field dependent magnetization corresponds to a superimposed precession motion of the orbiting electrons in the field  $\mathbf{B}$ . While a magnetization in this quasi classical picture must lead to an increase of the energy of the electronic system and hence is classified as diamagnetic response, in the quantum mechanical case the magnetic response in general can be partitioned into either diamagnetic or paramagnetic contributions. Such a paramagnetic magnetization has no quasi-classical counterpart, it however would correspond to a  $\mathbf{B}$  field dependent gain in angular momentum, leading to an energetic stabilization of the system. Also the partitioning into dia- and paramagnetic response contribution in general depends on the choice of the gauge, or in the particular case of a vector potential  $\mathbf{A}$  of the form  $\mathbf{A}_d(\mathbf{r}) = (\mathbf{r} - \mathbf{d}) \times \mathbf{B}$  on the choice of the gauge origin  $\mathbf{d}$ . A natural choice for the gauge origin, however is the origin of reference  $\mathbf{r}_0$  for the definition of the angular momentum (operator)  $\mathbf{l} = (\mathbf{r} - \mathbf{r}_0) \times \mathbf{p}$ , by the momentum (operator)  $\mathbf{p}$ , which serves also as centre of symmetry in case of non-trivial molecular symmetries and conveniently can be used as origin of the inner coordinate system of the molecule (then  $\mathbf{r}_0 = \mathbf{0}$ ). According to McWeeny's perturbation theoretic formulation<sup>6</sup> and orienting a unit strength magnetic field along the  $z$  axis:  $\mathbf{B} = (0, 0, 1)^T = \mathbf{B}_z$ , the paramagnetic part of the magnetically induced current density field  $\mathbf{J}_p^{\mathbf{B}_z}(\mathbf{r})$  is obtained by

$$\mathbf{J}_p^{\mathbf{B}_z}(\mathbf{r}) = -\frac{2ne}{m_e} \Re \int d\mathbf{s}_1 d\mathbf{x}_2 \dots d\mathbf{x}_n \Psi^{\mathbf{B}_z*}(\mathbf{x}_1, \dots, \mathbf{x}_n) \mathbf{p} \Psi_0(\mathbf{x}_1, \dots, \mathbf{x}_n) \quad (1)$$

with the  $n$  the number of electrons, the electronic charge  $-e$ , the electron mass  $m_e$ , and the ground state wave function  $\Psi_0$  that depends on spatial coordinates of the  $i$ -th electron  $\mathbf{r}_i$  and its spin coordinate  $s_i$  which are combined to the space-spin coordinate  $\mathbf{x}_i$  and the (purely imaginary) first order magnetic response contribution to the wave function

$$\Psi^{\mathbf{B}_z}(\mathbf{x}_1, \dots, \mathbf{x}_n) = -\frac{e}{2m} \sum_{j>0} \Psi_j \frac{\langle \Psi_j | \mathbf{l}_z | \Psi_0 \rangle}{\varepsilon_j - \varepsilon_0}, \quad (2)$$

using  $\mathbf{l}_z$  for the  $z$ -component of the (total) angular momentum operator. Alternatively an effective one-particle picture formulation can be easily obtained, resulting in an completely analogous expression for occupied-unoccupied orbital excitations. Thus the possibility of occurrence of a paramagnetic response contribution  $\mathbf{J}_p^{\mathbf{B}_z}(\mathbf{r})$  is determined by the condition

$$\frac{|\langle \Psi_j | \mathbf{l}_z | \Psi_0 \rangle|}{\varepsilon_j - \varepsilon_0} > 0, \quad (3)$$

which in turn can be interpreted as a selection rule for  $\mathbf{J}_p^{\mathbf{B}_z}(\mathbf{r})$  requiring the possibility of virtual excitations between  $\Psi_0$  and  $\Psi_j$  of rotational symmetry with respect to an axis parallel to  $z$  (the direction of the magnetic field  $\mathbf{B}_z$ ). The connection between paramagnetism and rotation to the best of our knowledge was pointed out for the first time by Steiner & Fowler<sup>7</sup>. According

to the Wigner-Eckart theorem we can formulate the selection rule, that the decomposition of the direct (tensor) product of the irreducible representations (IRs,  $\Gamma$ ) of the ground and excited states must contain the IR of the  $z$  component of the angular momentum operator:

$$\Gamma_{\mathbf{I}_z} \subseteq \Gamma_{\Psi_j} \otimes \Gamma_{\Psi_0}. \quad (4)$$

Also the terms and hence total paramagnetic currents in general will be the stronger the larger the integrals  $\left| \langle \Psi_j | \mathbf{I}_z | \Psi_0 \rangle \right|$  and the smaller the energy gaps  $\varepsilon_j - \varepsilon_0$  between the engaged states are. In this specific choice of gauge, that is a common gauge origin, one can introduce the terms of dia- and paratropicity<sup>8</sup>, which are referring to ring current contributions to the total current density vector field that are flowing either in classical direction or anti-classical direction around the gauge origin and with respect to the external magnetic field, thus giving rise to a dia- or paramagnetic induced magnetisation inside this ring current domain, respectively.

Thus representations of angular momentum components play a central role in our considerations. In the following we will see that there is an intimate connection between tensor squares of two-dimensional IRs and representations of angular momentum components in certain point groups.

### 3 Angular momentum in squares of degenerate IRs

A *point group* is a subgroup of  $O(3)$ , or from a more mathematical point of view, an abstract group together with a faithful representation of itself into  $O(3)$ . Thus two point groups can be isomorphic as abstract mathematical groups but be different representations at the same time (e.g.  $C_s$  and  $C_2$ ), and for that be different point groups. The reason we want to separate the discussion of the group from the discussion of its representation is that we naturally encounter several representations by the same group. A word of warning, while in mathematics a representation is of a group and acting on a vector space, placing the group first in order of importance, we instead talk of representations of vector spaces or of operators, by a group. This different phrasing is because the operators are what is more concrete in chemistry than the abstract groups.

The physical space  $\mathbb{R}^3$  upon which the group elements act, serves as the representation space implied by the concept of point group. Hence its axis  $(x, y, z)$  represent the algebraic generators of the physical quantities corresponding to operators or observables, which thereby can be analysed in terms of irreducible representations.

Once we have this representation  $\rho$  of physical space, we often want to describe its action on algebraically related spaces, such as direct sums, tensor spaces or dual spaces, or in the present case, angular-momentum space. Computing the representations of those more complex spaces from the initial representation of physical space can be described mathematically with the use of Schur functors. The functor that will interest us in order to describe the representation of the

angular momentum operator is the second exterior power :

If we have a change of variable represented by an orthogonal linear map  $\mathbf{r}' = U\mathbf{r}$ , then  $\nabla' = U\nabla$  because  $U$  is orthogonal, so that when transforming the angular momentum operator, we get  $\mathbf{L}' = -i\hbar(\mathbf{r}' \times \nabla') = -i\hbar(U\mathbf{r} \times U\nabla) = (U \times U)\mathbf{L}$  where  $U \times U$  (which can also be written  $U \wedge U$ ,  $[U \otimes U]$  or  $Alt^2(U)$ ) is the application of the second exterior power to  $U$ . Finally since a representation is nothing but a family of orthogonal linear maps, we can also apply Schur functors to representations, so that if  $\rho$  is a representation of the physical space,  $Alt^2(\rho)$  is the representation of the angular momentum operator.

Once we have identified this relationship, we gain the advantage of having computation rules, such as  $Alt^2(\rho_1 \oplus \rho_2) = Alt^2(\rho_1) \oplus Alt^2(\rho_2) \oplus \rho_1 \otimes \rho_2$ . The symmetric square functor  $Sym^2$  is also of interest, it satisfies the same rule, and we have the functor decomposition  $\rho \otimes \rho = Sym^2(\rho) \oplus Alt^2(\rho)$ . Finally, if  $\Gamma$  is a real irreducible representation by a group  $G$ , then  $Sym^2(\Gamma)$  always has exactly one totally symmetric  $\Gamma_0$  component in its decomposition, so that for any two dimensional real irreducible representation  $E$ ,

$$E \otimes E = Alt^2(E) \oplus \Gamma_0 \oplus \rho_q; \quad dim(\Gamma_0) = 1, \quad dim(\rho_q) = 2. \quad (5)$$

We also make a note that functors commute with restrictions. If  $F$  is a functor,  $\rho$  a representation by a group  $G$ , and  $H$  a subgroup of  $G$ , then for any  $h \in H$ ,  $F(\rho|_H)(h) = F(\rho|_H(h)) = F(\rho(h)) = (F(\rho))(h) = (F(\rho))|_H(h)$ , so that  $F(\rho|_H) = (F(\rho))|_H$ . This works exactly the same way for bifunctors such as direct sums or tensor products of two representations.

We investigate what this entails when we look at the representation of the angular momentum operator of point groups. The main result we will want to prove is that the  $Alt^2$  functor has a tendency to output the same (irreducible) representation when you give as input different irreducible representations of the same dimension.

We will now be revisiting the classification of point groups by paying more attention to the irreducible representations of their underlying groups. The family of point groups can be partitioned into three subfamilies ( $\mathcal{K}_{aaa}$ ,  $\mathcal{K}_{ae}$ ,  $\mathcal{K}_t$ ) according to the reducibility of their implied faithful three-dimensional representations of physical space :

1. Point groups whose faithful representations decompose into three components, so that they embed in  $O(1) \times O(1) \times O(1)$ , *i.e.* groups that have no axis of rotation of order  $n > 2$  (family  $\mathcal{K}_{aaa}$ ). In detail  $\mathcal{K}_{aaa} = \{C_1, C_2, C_{2v}, C_s, C_{2h}, D_2, D_{2h}, C_i\}$ .
2. Point groups whose faithful representations decompose in two irreducible components but not three, so they embed in  $O(1) \times O(2)$ , *i.e.* groups that have a unique main axis of

rotation of highest order  $n > 2$  (family  $\mathcal{K}_{ae}$ ). In detail  $\mathcal{K}_{ae} = \{C_3, C_4, \dots, C_{3v}, C_{4v}, \dots, C_{3h}, C_{4h}, \dots, D_3, D_4, \dots, D_{3h}, D_{4h}, \dots, D_{2d}, D_{3d}, \dots, S_4, S_6, \dots\}$ .

3. Point groups whose faithful representations are irreducible, *i.e.* groups that have more than one axis of rotation of order  $n > 2$ , which are also called isometric groups (family  $\mathcal{K}_t$ ). In detail  $\mathcal{K}_t = \{T, T_d, T_h, O, O_h, I, I_h\}$ .

It is not obvious that this partition defined in terms of a specific representation, carries down to the level of abstract groups independent of specific representations. We note that this is not true in general for abstract groups represented in  $O(n)$  for  $n > 3$ .

In the following we use the Mulliken conventions of  $A, B$  for one-dimensional,  $E$  for two-dimensional,  $T$  for three-dimensional irreducible representations over  $\mathbb{R}$ ,  $\rho$  for a general representation,  $\Gamma$  for an irreducible one and  $\Gamma_0$  for the trivial (= totally symmetric) representation. Now, we consider a point group from the first two families, whose representation is reducible, such that it decomposes into a direct sum  $\rho = A \oplus E$ .

An equivalent property is that the representation has a unique main symmetry axis, and then this axis is the subspace acted on by  $A$ : Let  $n$  be the maximum order of a rotation of the representation and consider the set of all the axis of the order  $n$  rotations. The group acts on this set of axis as the group acts by conjugation on the rotations: if a line  $l$  is the axis of a rotation  $\rho(g)$  and  $h \in G$ , then  $\rho(hgh^{-1})$  is a rotation whose axis is  $\rho(h)(l)$ . If there is only one such axis  $l$  (called the main symmetry axis), it means that  $\rho(h)(l) = l$  for all  $h \in G$ , that is  $l$  is a subspace stabilized by  $G$ , so  $\rho$  is decomposes as a direct sum of the action on  $l$  and the action on its orthogonal. We will thus call this  $l$  (or  $A$ 's underlying vector space) the  $z$ -axis and its orthogonal (or  $E$ 's vector space) the  $(x, y)$ -plane.

In this  $\mathcal{K}_{ae}$  family, the angular momentum operator  $Alt^2(\rho)$  decomposes into  $Alt^2(\rho) = Alt^2(A) \oplus Alt^2(E) \oplus A \otimes E$ . Since  $A$  is one dimensional,  $Alt^2(A)$  is zero-dimensional and can be omitted:  $Alt^2(\rho) = Alt^2(E) \oplus A \otimes E$ .

Thus for point groups from  $\mathcal{K}_{ae}$  the (quantum mechanical) angular momentum (operator) decomposes into a one dimensional, hence irreducible, representation on the rotations around the  $z$ -axis  $\Gamma_{\hat{l}_z} = Alt^2(E)$  (which is also the anti-symmetric square of the representation of the  $(x, y)$ -plane) and a two-dimensional representation  $\Gamma_{\hat{l}_{x,y}} = A \otimes E$  on the rotations whose axis lie in the  $(x, y)$ -plane.

Moreover,  $Sym^2(E)$  here further decomposes into  $\Gamma_0 \oplus \rho_q$  where  $\Gamma_0$  is the totally symmetric IR and  $\rho_q$  is some two-dimensional representation. In summary for groups from  $\mathcal{K}_{ae}$  we have:

$$E \otimes E = \underbrace{\Gamma_{\hat{l}_z}}_{=Alt^2(E)} \oplus \underbrace{\Gamma_0 \oplus \rho_q}_{=Sym^2(E)}; \quad \dim(\Gamma_0) = \dim(\Gamma_{\hat{l}_z}) = 1, \dim(\rho_q) = 2. \quad (6)$$

We now want to prove the following property of their underlying abstract group, that given two (two-dimensional real irreducible) representations  $E_1, E_2$  of point groups from  $\mathcal{K}_{ae}$ , then  $Alt^2(E_1) = Alt^2(E_2)$ , so that

$$\forall G \in \mathcal{K}_{ae}, \forall E \in Irrep(G, 2), Alt^2(E) = \Gamma_{\hat{iz}} \quad (7)$$

We start with finding out the possible underlying abstract groups from the families  $\mathcal{K}_{aaa}$  and  $\mathcal{K}_{ae}$  and show they belong to one of the four families  $C_n, D_n, C_n \times C_2$  and  $D_n \times C_2$ . It is easy to see that  $C_{nv}$  and  $D_n, C_{nh}$  and  $C_n \times C_2, D_{nh}$  and  $D_n \times C_2, D_{nv}$  and  $D_{2n}$ , and  $S_{2n}$  and  $C_{2n}$  are isomorphic. Then let  $G$  be a finite group faithfully represented in  $O(1) \times O(2)$ . This means we have two maps  $\phi_i : G \rightarrow O(i)$  such that  $G$  is a subgroup of  $G' = \phi_1(G) \times \phi_2(G)$ . If  $\phi_2$  is not an isomorphism of  $G$  to  $\phi_2(G)$ , then  $|G'| \geq |G| > |\phi_2(G)|$ . But since  $|G'|/|\phi_2(G)| = |\phi_1(G)|$  can only be 1 or 2, we must have  $|\phi_1(G)| = 2$  and  $|G'| = |G|$ , so that  $G = G'$ . This proves that  $G$  is isomorphic to either a finite subgroup of  $O(2)$ , or to a product of one with  $C_2$ .

We now prove the property for the finite subgroups  $C_n$  and  $D_n$  of  $O(2)$ .  $C_n$  are abelian groups, so their complex irreducible characters are all one-dimensional. Given a choice of generator of  $g \in C_n$ , for each  $n$ th root of unity  $\zeta$  there is one character  $\chi_\zeta$  such that  $\chi_\zeta(g) = \zeta$ . The real irreducible representations are obtained by pairing  $\chi_\zeta$  with  $\chi_{\bar{\zeta}}$  when  $\zeta$  is not real and building their direct sum. Then,  $Alt^2(\chi_\zeta \oplus \chi_{\bar{\zeta}}) = \chi_\zeta \otimes \chi_{\bar{\zeta}} = \chi_1 = 1$ .

The dihedral groups  $D_n$  are generated by two elements  $r$  and  $s$  subject to the relations  $r^n = s^2 = rsrs = e$ . They have complex two-dimensional irreducible representations  $\rho_k$ , given by the assignments

$$r \mapsto \begin{pmatrix} \cos \frac{2k\pi}{n} & -\sin \frac{2k\pi}{n} \\ \sin \frac{2k\pi}{n} & \cos \frac{2k\pi}{n} \end{pmatrix}, \text{ and } s \mapsto \begin{pmatrix} 1 & 0 \\ 0 & -1 \end{pmatrix}, \text{ for } 0 < k < n/2.$$

Then  $Alt^2(\rho_k)(r) = (1)$  and  $Alt^2(\rho_k)(s) = (-1)$ , which are independent of  $k$ .

This proves the claim for the  $C_n$  and  $D_n$  families. As for the  $C_n \times C_2$  and  $D_n \times C_2$  families, their irreducible representations are tensor products of one irreducible representation of each. Since we are in dimension 2, for any  $E$  representation of  $C_n$  or  $D_n$  and  $A$  representation of  $C_2$ , we have  $Alt^2(E \otimes A) = Alt^2(E) \otimes (A \otimes A) = Alt^2(E) \otimes \Gamma_0$ , which is independent of the choice  $E$  and  $A$ .

Note that the determination of the irreducible representations of those groups show that our classification of point groups is also a classification at the level of groups : we have shown in all cases that there was no three-dimensional irreducible representation of  $G$ , so in particular that those families  $\mathcal{K}_{aaa}$  and  $\mathcal{K}_{ae}$  of groups are disjoint from the family  $\mathcal{K}_t$ . Moreover, if  $n \geq 3$  then  $G$  cannot be faithfully represented by a direct sum of three one dimensional representations as then  $G$  cannot have any element of order higher than two. Thus any faithful representation of those groups in  $O(3)$  has an  $A \oplus E$  shape, and has a (unique) main axis of symmetry. Those

groups form the family  $\mathcal{K}_{ae}$ . Finally, if  $n \leq 2$  then there are no two-dimensional irreducible representation of  $G$ , so those groups are the  $\mathcal{K}_{aaa}$  family. In their case, the choice of a  $z$ -axis needs more than just algebraic considerations.

Consider now a point groups from the family  $\mathcal{K}_t$  (*i.e.* an isometric point group), it comes with a faithful irreducible representation  $T$  into  $O(3)$ . Such a point group cannot distinguish between the three coordinate axis  $x, y$  and  $z$ .

Then the angular momentum representation  $\Gamma_l = \text{Alt}^2(T)$  is irreducible. For three-dimensional representations,  $\text{Alt}^2(\text{Alt}^2(T)) = \det(T) \otimes T$ , so if  $\text{Alt}^2(T)$  was reducible, the reducibility would carry over to  $\det(T) \otimes T$ , and then by tensoring again with  $\det(T)$ , to  $T$  itself.

Among the cubic point groups, this is a subfamily of the isometric point groups consisting of  $T, T_d, T_h, O$  and  $O_h$ , a similar property is true : if  $T_1$  and  $T_2$  are two irreducible three-dimensional representations, then  $\text{Alt}^2(T_1) = \text{Alt}^2(T_2) = \Gamma_l$ . This is because in every case, there is a one dimensional representation  $A$  such that  $T_2 = A \otimes T_1$ , so that  $\text{Alt}^2(T_2) = \text{Alt}^2(T_1) \otimes A \otimes A = \text{Alt}^2(T_1)$ . Among the icosahedral groups ( $I, I_h$ ), this is no longer true. Here also the symmetric square  $\text{Sym}^2(T)$  further decomposes into  $\Gamma_0 \oplus \rho_q$  where  $\rho_q$  is some five-dimensional representation.

A summary of all (non-linear) point groups, their  $n > 1$  dimensional IRs (over  $\mathbb{R}$ ), their  $\text{Alt}^2$  functors and the respective  $\Gamma_{1_z}$  IR is given in the Supplementary Information section in table 1.

The group theory based considerations in the next section of branchings of degenerate electronic levels will allow us to connect this symmetry “selection rule” with degeneracy of levels and we will see that double degeneracy plays the central role.

## 4 Distortions

Distorting a molecule from a higher to a lower symmetric structure leads to a restriction of the representations of molecular eigenstates to a subgroup  $H$  of  $G$ , which can change the shape of its irreducible decomposition (this is called ‘descent in symmetry’ in chemistry and ‘branching representation theory’ in mathematics).

Consider a point group  $\mathcal{H} \subset \mathcal{G}$ , and a two dimensional representation  $E$  by  $\mathcal{G}$ . If the restriction of  $E$  to  $\mathcal{H}$  ( $= E|_{\mathcal{H}}$ ) branches into a direct sum of two one-dimensional representations of  $\mathcal{H}$ ,

$$E|_{\mathcal{H}} = A_{\alpha} \oplus A_{\beta} \quad (8)$$

then

$$\text{Alt}^2(E)|_{\mathcal{H}} = \text{Alt}^2(E|_{\mathcal{H}}) = A_{\alpha} \otimes A_{\beta}. \quad (9)$$



If  $E$  was the representation of the point group  $\mathcal{G}$  on the  $(x, y)$ -plane, then

$$\Gamma_{\hat{L}_z}|_{\mathcal{H}} = \text{Alt}^2(E)|_{\mathcal{H}} = A_\alpha \otimes A_\beta. \quad (10)$$

The angular momentum representation of  $\mathcal{H}$  on the rotations around the  $z$ -axis is the tensor product of the two representations  $A_\alpha, A_\beta$ .

This implies that if an  $E$ -type IR in a non-isometric point group is restricted to a subgroup such that it splits into two non-degenerate hence one-dimensional IRs, then the direct product of these two one-dimensional representations is exactly the representation of the  $z$ -component of the angular momentum operator. This is an essential result.

A large part of actual molecular examples for JT distortions are second order JT cases. In the next section we show that these considerations can be extend to a certain subset of second order JT cases.

## 5 'Primoid' second order JT systems

We adopt in the following a simplistic view on the Jahn-Teller-Effect<sup>1</sup> based on the original idea from Landau and Teller where distortions were considered in the form of small perturbations and based on a specific situation of electronic degeneracy and we are focusing only on the basic integrals occurring in the perturbation expansion<sup>10</sup> of the molecular energy with respect to a deviation (or distortion)  $Q$  from the minimum geometry on the adiabatic potential energy surface, which in general may be regarded as some symmetry adapted local nuclear coordinate system like a system of vibrational normal modes. In that sense the occurrence of a first order JT distortion is determined by the size of the first order coefficients in  $Q$ :

$$\langle \Psi_0 | \frac{d\hat{H}}{dQ} | \Psi_0 \rangle \quad (11)$$

with the ground state wave function  $\Psi_0$ , while second order JT distortions are determined by the negative components of the second order coefficients<sup>10</sup>

$$\sum_{i>0} \frac{\left| \langle \Psi_0 | \frac{\partial \hat{H}}{\partial Q} | \Psi_i \rangle \right|^2}{\varepsilon_0^0 - \varepsilon_i^0} \quad (12)$$

with the virtual state wave functions  $\Psi_i$ , and the corresponding unperturbed state energies  $\varepsilon_j^0$  (for  $j = 0, i$ ).

---

<sup>1</sup>As a starting point for a deeper understanding and a contemporary view on the JT-effect we refer the reader to I. B. Bersuker's introductory text "Recent Developments in the Jahn-Teller Effect theory"<sup>9</sup>.

The JTT implies that for a twofold degenerate one-electron state  $\psi_0$  ( $E$  type) in a non-linear point group  $G$  a non-totally symmetric distortion mode  $Q$  exists such that according to expression 11 we have  $\Gamma_Q \subseteq \Gamma_{\psi_0}^* \otimes \Gamma_{\psi_0}$ .

Now an occupation of  $\psi_0$  with a second electron will give rise to various possible combinations of occupied and virtual two electron state ( $\Psi_0$  and  $\Psi_i$ ) symmetries:  $\Gamma_{\Psi_0}, \Gamma_{\Psi_i} \subset \Gamma_{\psi_0} \otimes \Gamma_{\psi_0} = \Gamma_0 \oplus \text{Alt}^2(E) \oplus \rho_q$  (with eq. 6). From those one can choose  $\Gamma_{\Psi_0} = \Gamma_0$  and  $\Gamma_{\Psi_i} = \Gamma_Q$ , yielding, as the comparison with expression 12 suggests  $\Gamma_Q \subseteq \Gamma_0^* \otimes \Gamma_Q$ , such that a second order JT distortion by the mode  $Q$  is possible. Such a choice we call “**primoid** second order JT system”.

By this two electron wave function construction both  $\Psi_0$  and the virtual state  $\Psi_i$  can only be in the decomposition of  $E \otimes E$ , which together with the restriction to cases where JT causes only small structural perturbations can warrant that the energy denominator in expression 12 is not too large.

For a counter example of a *non-primoid* second order JT case, consider  $\text{Si}_4\text{F}_4$  in the abelian  $D_{2h}$  symmetry<sup>11</sup> which distorts via a  $B_{1g}$  mode to  $C_{2h}$ , or similarly  $\text{Si}_2\text{Ge}_2\text{F}_4$  which distorts from  $D_{2h}$  via  $C_{2h}$  to  $C_s$ . In general, all cases of second order Jahn-Teller distortion which are of an idealized (or highest possible) point group symmetry that possesses no degenerate IRs over  $\mathbb{R}$ , are non-primoid second order Jahn-Teller cases.

## 6 JT and paramagnetism in point groups from $\mathcal{K}_{ae}$

All point groups  $G$  in the family  $\mathcal{K}_{ae}$  are represented by at least one two-dimensional IR over  $\mathbb{R}$ , say  $E$  and in these point groups  $\text{Alt}^2(E)$  represent the  $z$ -component of the quantum mechanical angular momentum operator. Molecular systems in electronic states represented by  $E$  are due to their degeneracy prone to a first order JT distortion. If such a distortion to a subgroup  $H$  of  $G$  occurs then  $E$  branches into two one-dimensional representations, say  $A_\alpha$  and  $A_\beta$ . The corresponding lower lying electronic state say  $A_\alpha$  eventually will become the ground state (or a SOMO or HOMO orbital in the effective one-particle picture) while the higher lying state  $A_\beta$  will become some virtual state (or a UMO or possibly the LUMO depending on the size of the distortion). Then and especially if the distortion is not too large, such that the energy difference between occupied and virtual states will not become too large, the system becomes by virtue of the symmetry selection rule for paratropic currents (eqns. 1 and 3) strongly susceptible to induced paratropic currents (note also that according to eq. 10  $A_\alpha \otimes A_\beta = \Gamma_{1_z}$ ). In this way all JT first order cases arising from point groups  $G$  in the family  $\mathcal{K}_{ae}$ , that is all non-isometric first order JT cases, since the point groups in family  $\mathcal{K}_{aaa}$  are not represented by non-one-dimensional IRs, inherently are prone to paramagnetism.

Since this result is based on group theoretical considerations it can be seen as a completely general symmetry property that combines structure and magnetic response. Similar as the dipole transition rule which gives a general symmetry property of the molecular response with respect to any diopole fields. Like such spectroscopic selection rules, the predictivity is of course limited by the fact that we deal merely with symmetry rules which are completely independent of the peculiar quantitative electronic properties of a molecule under investigation. But also similar to these selection rules the principle might serve as a basis for the understanding of the phenomenon of antiaromaticity in a very general sense.

It is very important to note that these considerations are not restricted to the first order JT effect since this is bound to open shell systems, and the most important examples for antiaromaticity like 1,3-cyclobutadiene are closed shell cases. From the definition of the *primoid* second order JT case it follows immediately that there is the very same connection between symmetry and paratropic response currents. One example is 1,3-cyclobutadiene, that goes back to states derived from a doubly occupied doubly degenerate orbital.

We now can formulate the main result of this work, as is announced in the introduction:

*First order and primoid second order JT distorted molecules out of non-isometric point groups are prone to paramagnetic current susceptibility parallel to the main axis of symmetry*

and add that

*This is the symmetry principle of antiaromaticity.*

In the following we will discuss four representative examples for molecules, each of them reflecting a slightly different situation in hindsight to the symmetry rule for antiaromaticity.

## 7 Examples

### 7.1 C<sub>4</sub>H<sub>4</sub>

1,3-Cyclobutadiene (C<sub>4</sub>H<sub>4</sub>) is such a prominent example for antiaromaticity that it is mentioned in the IUPAC definition (see ref.<sup>4,5</sup> and the SI for a full quote). Details on its symmetry, electronic states and the nature of the Jahn-Teller distortion have been worked out by Nakamura & co-workers<sup>12</sup> in the framework of a MCSCF study. It is a case where for the full  $D_{4h}$  symmetry we have double occupation of the doubly degenerate  $e_g$  orbitals ( $e_g^2$ ), which results in purely non-degenerate electronic states, the first four of which are in energetically ascending order  $^1B_{1g}$ ,  $^3A_{2g}$ ,  $^1A_{1g}$ ,  $^1B_{2g}$ . Hence, this is a prototypical example for a primoid second order

Jahn-Teller case.

Formally removing one electron yields the  $[\text{C}_4\text{H}_4]^+$  cation and a  ${}^2E_g$  ground state. To check the possibility of a non-zero integral term 11, thus the possibility of existence of a distortional mode  $Q$  leading to an energetic stabilization, which is a condition for a first order JT effect, we need to decompose  $E_g \otimes E_g$  into a direct sum of IRs. This yields

$$E_g \otimes E_g = A_{1g} \oplus [A_{2g}] \oplus B_{1g} \oplus B_{2g} \quad (13)$$

The only permissible distortion mode symmetry (as must be checked separately) here is  $B_{1g}$ . Now distortion of  $D_{4h}$  along this JT predicted  $B_{1g}$  mode leads to  $D_{2h}$  symmetry, opening in principle two possibilities for distortion, that is the rhombic or rectangular geometry, and assuming the latter, with it a splitting of the degenerate  $E_g$  level into the two one-dimensional levels  $B_{2u}$  and  $B_{3u}$ .

Since  $D_{4h}$  is a non-isometric point group (case  $\mathcal{K}_{ae}$ ) and  $E_g$  is a degenerate level we know according to eq. 6 that  $E_g \otimes E_g$  contains the IR for the  $z$ -component of the angular momentum  $\Gamma_{1z}$ , which in  $D_{4h}$  is  $A_{2g}$ . Moreover from eq. 7 follows that this is  $\Gamma_{1z} = \text{Alt}^2(E_g) = [E_g \otimes E_g] = A_{2g}$ . According to eq. 10 in the new group  $D_{2h}$  the IR for  $1_z$  is contained in the direct product of the two branches of  $E_u$ . That this is indeed the case shows a quick check: in  $D_{2h}$  we have  $B_{2u} \otimes B_{3u} = B_{1g}$ , which is identical to  $\Gamma_{1z}$  in this group.

As we have identified  $\text{C}_4\text{H}_4$  by its orbital structure as a (potential) primoid second order JT case, by recursion to the hypothetical  $[\text{C}_4\text{H}_4]^+$  case we could easily identify the symmetry of the  $Q$  mode that could be operational in a second order JT effect in  $\text{C}_4\text{H}_4$ . And in addition by the arguments from above we know that in the “real” two electron state case  $e_g^2$  there will be occupied-virtual transitions of  $\Gamma_{1z}$  symmetry available in the accordingly distorted  $\text{C}_4\text{H}_4$  case.

We can verify this as well: Eq. 13 shows all permissible two electron states from the  $e_g^2$  occupation. Now as a matter of fact the ground state turns out to be of  ${}^1B_{1g}$  symmetry and out of the virtual states given by the remaining three terms of eq. 13 again only a virtual transition to the  ${}^1A_{1g}$  state has a symmetry that is in accordance with a permissible distortional coordinate  $Q$  (see  $[\text{C}_4\text{H}_4]^+$  case), that is

$$B_{1g} \otimes A_{1g} = B_{1g}. \quad (14)$$

So both models predict of course the same symmetry of distortion  $Q$  out of  $D_{4h}$  to  $D_{2h}$ . To find the by virtue of the “primoid” argument predicted virtual transition of  $\Gamma_{1z}$  symmetry we have to restrict all terms on the right side of eq. 13 to the subgroup  $D_{2h}$ . This gives

$$(A_{1g} \oplus A_{2g} \oplus B_{1g} \oplus B_{2g})|_{D_{2h}} = A_g \oplus B_{1g} \oplus A_g \oplus B_{1g} \quad (15)$$

Since thus the ground state “branches” from  $B_{1g}$  to  $A_g$ , for example a virtual transition  $A_g \rightarrow B_{1g}$  is available which is obviously of  $B_{1g}$  symmetry and, that as we have used already above, is identical to  $\Gamma_{1z}$  in  $D_{2h}$ .

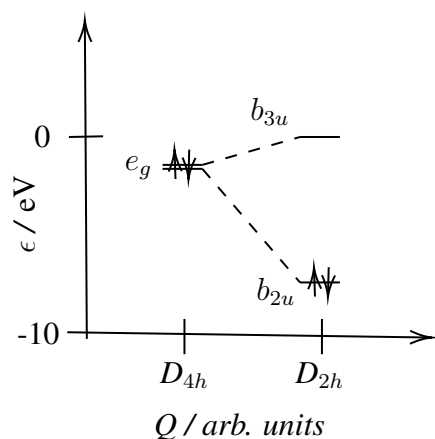
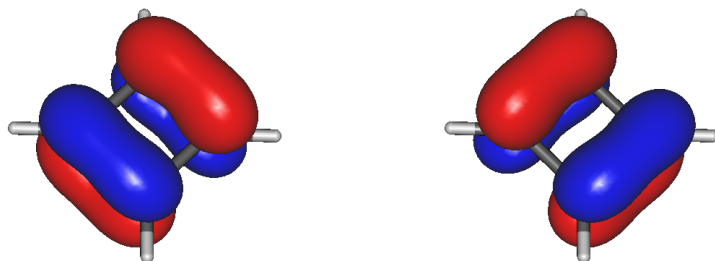


Figure 1: Frontier orbital energies  $\varepsilon$  for the ground state saddle point ( $D_{4h}$ ) or minimum structure ( $D_{2h}$ ) calculated at the generalized valence bond - perfect pairing (GVB(PP)/TZVPP) level of theory for cyclooctatetraene ( $C_4H_4$ ). Level splitting upon distortion  $Q$  from  $D_{4h}$  to the  $D_{2h}$  minimum is indicated by the dashed lines. The distortion from  $D_{4h} \rightarrow D_{2h}$  is a *primoid* second order Jahn-Teller (JT) distortion via a  $b_{1g}$  mode. The direct products  $e_g \otimes e_g$  and  $b_{2u} \otimes b_{3u}$ , the latter corresponding to the paramagnetic virtual excitation, contain or are the IR for the  $z$ -component of the angular momentum operator. The molecule in the  $D_{4h}$  saddle point configuration shows a much stronger paramagnetic response than the  $D_{2h}$  minimum structure (compare Fig. 3). but both are classified as antiaromatic.

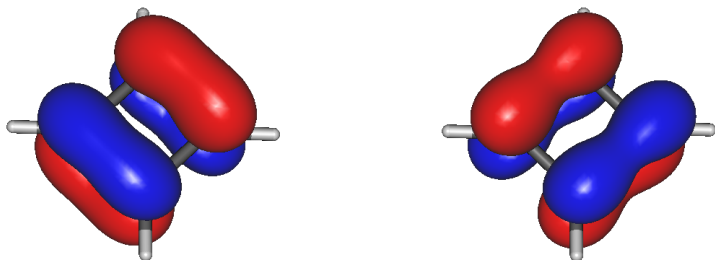
So we have shown how the argument of prediction of virtual transitions of  $\Gamma_{1_z}$  symmetry, that is paramagnetic response, for the primoid second order JT case  $C_4H_4$  (out of non-isometric point groups) works. Calculations show (see SI for details) that we can expect a double bond localization, or at least a splitting of C-C distances from 1.426 Å ( $D_{4h}$ ) to 1.552 and 1.324 Å. The weight of the second configuration is about 4% at the  $D_{2h}$  minimum structure, thus it is safe to use a single reference method for calculation of the magnetically induced ring currents (see SI for details). The integral of the total global current susceptibility amounts to -22.4 nA/T paratropic total current at HF/VTZ level of theory.

For the aromatic benzene we find diamagnetic current contributions of about +20 nA/T. One might say  $C_4H_4$  is as paramagnetic as benzene is diamagnetic (but one should note that there are paramagnetic contributions to the benzene currents as well and these are of a size of about -9 nA/T)<sup>13</sup>.

$C_4H_4$  is the classical example for antiaromaticity, in agreement with that we find that its ground state geometry is derived from, in this case, a primoid second order Jahn-Teller distortion out of a point group of the family  $\mathcal{K}_{ae}$ , it has a small HOMO-LUMO gap and thus inevitable as a consequence of the latter two arguments shows a strong paramagnetic response with respect to a magnetic field  $\mathbf{B}$  parallel to the original  $C_4$  axis.



(a) Highest occupied molecular orbital (HOMO) in the  $D_{4h}$  saddle point structure. The two-fold degenerate orbital is represented by the  $e_g$  IR.



(b) HOMO (left) and lowest unoccupied molecular orbital (LUMO, right) in the  $D_{2h}$  minimum structure. The HOMO is represented by  $b_{2u}$ , the LUMO by the  $b_{3u}$  IR.

Figure 2: Frontier orbitals of the electronic ground state in  $C_4H_4$  at different symmetries, calculated at the GVB(PP)/TZVPP level of theory, displayed as isosurfaces at densities of 0.066.

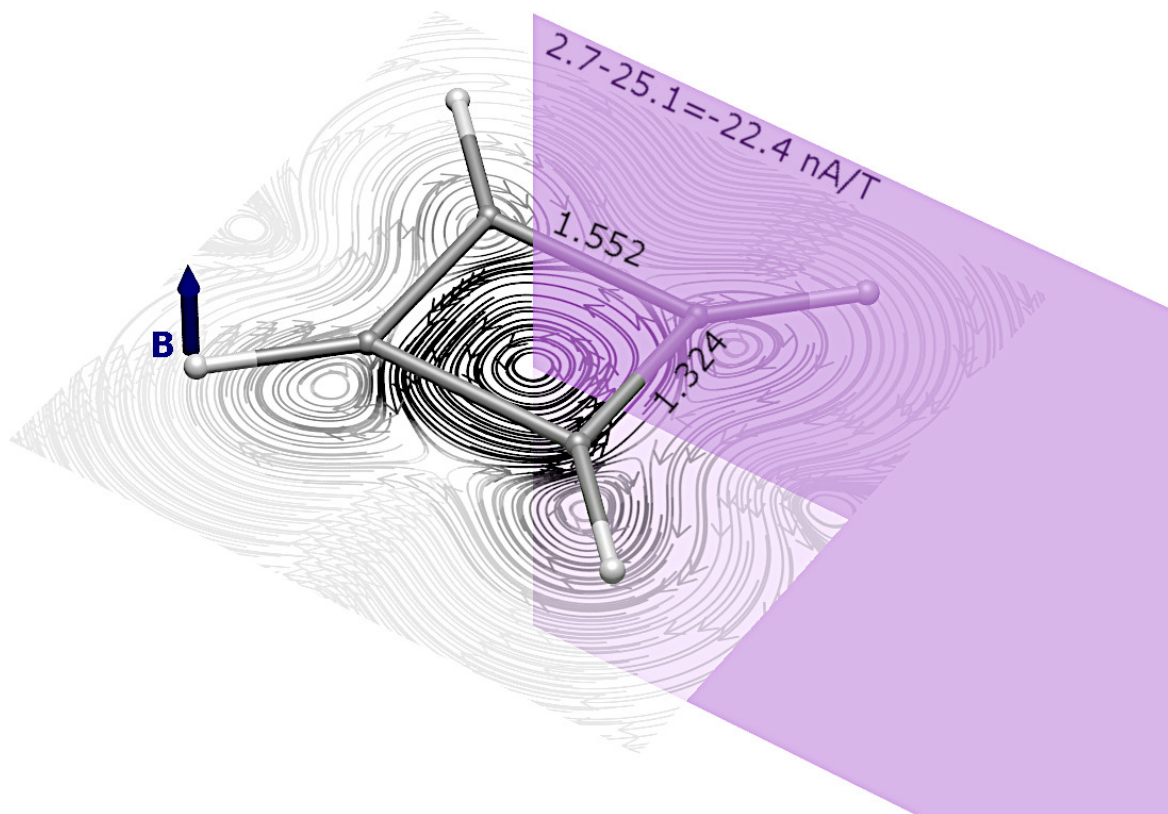


Figure 3:  $D_{2h}$  electronic ground state, minimum structure (distances given in units of Å) of  $C_4H_4$ , and stream line plot of magnetically induced (field direction indicated by the blue arrow) currents at a plane 0.5 Å, below the molecular plane. Integration of currents flowing through the purple surface yields a global molecular ring current of -22.4 nA/T (paratropic).

## 7.2 $C_8H_8$

Another example from the compound class of the n-annulenes is cyclooctatetraene ( $C_8H_8$ ) which is similar to  $C_4H_4$  in that it represents also a primoid second order JT case, but as we will see shows some quantitative difference in its paramagnetic response.

The idealized  $D_{8h}$  symmetry is not observed as a ground state minimum<sup>14</sup> due to a primoid second order JT distortion ( $e_u^2$  case). Also here we observe a  $B_{1g}$  distortion to a  $D_{4h}$  structure, which turns out to be no minimum structure either as it undergoes another second order JT distortion along a  $B_{1u}$  mode to a  $D_{2d}$  symmetric minimum structure. As the first distortion is



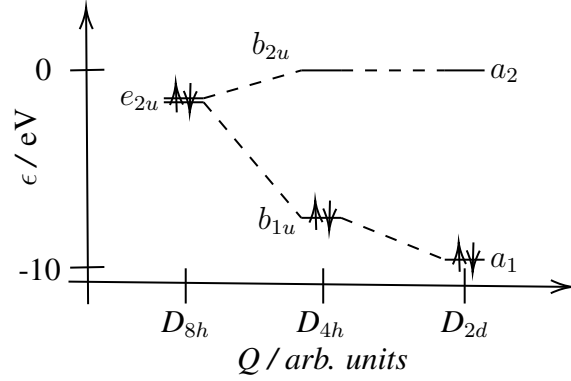
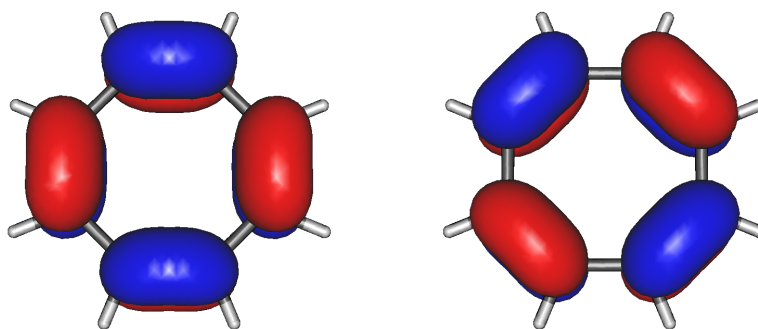


Figure 4: Frontier orbital energies  $\varepsilon$  for the ground state saddle point ( $D_{8h}$  of second order,  $D_{4h}$  of first order) or minimum structures ( $D_{2d}$ ) calculated at the generalized valence bond - perfect pairing (GVB(PP)) level of theory for cyclooctatetraene ( $C_8H_8$ ). Level splitting upon distortion  $Q$  from  $D_{8h}$  via  $D_{4h}$  to the  $D_{2d}$  minimum is indicated by the dashed lines. The first distorting  $D_{8h} \rightarrow D_{4h}$  is a *primoid* second order Jahn-Teller (JT) distortion via a  $b_{1g}$  mode, the second one is a non-primoid JT distortion via a  $b_{1u}$  mode. All three direct products  $e_{2u} \otimes e_{2u}$ ,  $b_{1u} \otimes b_{2u}$ , and  $a_1 \otimes a_2$ , the latter two corresponding to the paramagnetic virtual excitation, contain or are the IR for the  $z$ -component of the angular momentum operator. Virtual excitations represented by the terms given in expression 12 are not only decreasing by virtue of the increasing energy denominator but also due to the decreasing overlap integral in the numerator. Thus the molecule in the  $D_{4h}$  saddle point configuration shows a much stronger paramagnetic response than the  $D_{2d}$  minimum structure (compare Fig. 6).

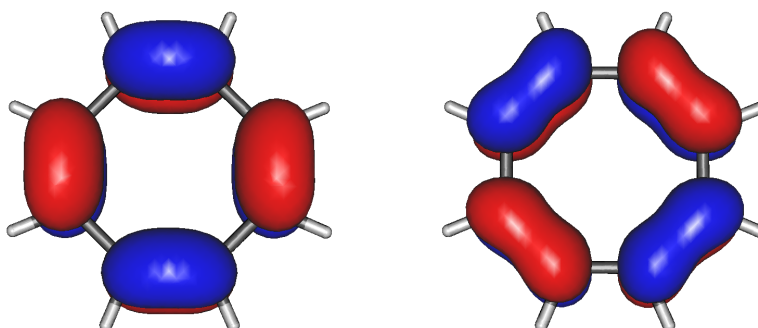
of primoid type we know that in  $D_{4h}$ , the IR  $\Gamma_{1z}$  will be the tensor product of the branches of the  $e_u$  orbitals. As these are  $b_{1u}$  and  $b_{2u}$  and  $b_{1u} \otimes b_{2u} = a_{2g}$  and  $\Gamma_{1z} = a_{2g}$  in  $D_{4h}$  we find our symmetry rule confirmed. Now since  $C_8H_8$  undergoes another second order JT distortion into  $D_{2d}$  we still find

$$\begin{aligned} (b_{1u} \otimes b_{2u})|_{D_{2d}} &= a_{2g}|_{D_{2d}} \\ b_{1u}|_{D_{2d}} \otimes b_{2u}|_{D_{2d}} &= a_2 \\ a_1 \otimes a_2 &= a_2 \end{aligned}$$

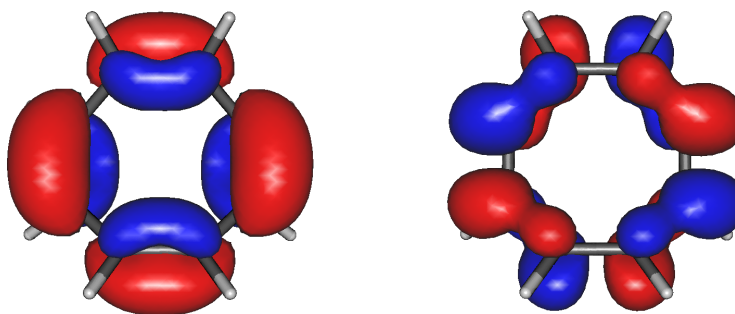
And  $a_2$  indeed represents  $\Gamma_{1z}$  in  $D_{2d}$  so that our prediction that the levels that were branching out of ( $e_u$ ) in this sequence of JT distortions relate to each other in  $\Gamma_{1z}$  manner and thus we again predict paramagnetic response for the  $D_{2d}$  minimum of  $C_8H_8$ , since we started from a non-isometric point group symmetry.



(a) Highest occupied molecular orbital (HOMO) in the  $D_{8h}$  double saddle point structure. The two-fold degenerate orbital is represented by the  $e_{2u}$  IR.



(b) HOMO (left) and lowest unoccupied molecular orbital (LUMO, right) in the  $D_{4h}$  double saddle point structure. The HOMO is represented by  $b_{1u}$ , the LUMO by the  $b_{2u}$  IR.



(c) HOMO ( $a_1$ , left) and LUMO ( $a_2$ , right) in the  $D_{2d}$  minimum structure.

Figure 5: Frontier orbitals of the electronic state in  $C_8H_8$  at different symmetries, calculated at the GVB(PP)/TZVPP level of theory, displayed as isosurfaces at densities of 0.05.

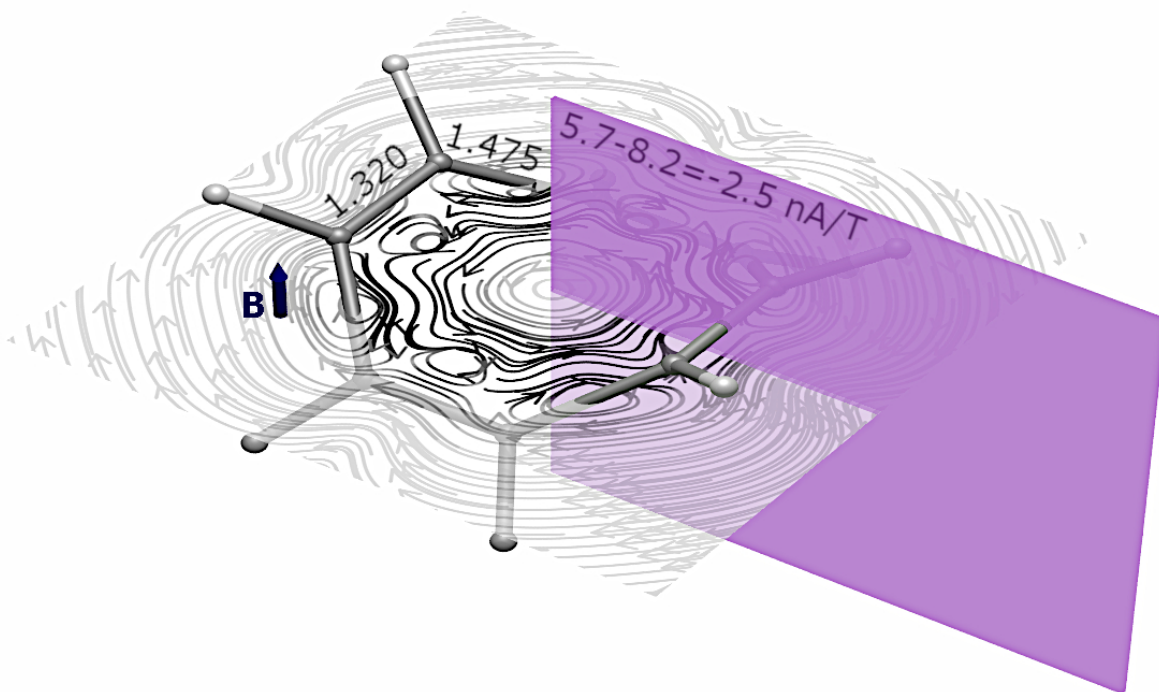


Figure 6:  $D_{2d}$  electronic ground state, minimum structure (distances given in units of Å) of  $C_8H_8$ , and stream line plot of magnetically induced (field direction indicated by the blue arrow) currents in the average molecular plane ( $x, y$ -plane). Integration of currents flowing through the purple surface yields a global molecular ring current of  $-2.5$  nA/T (purely paratropic contribution).

In contrast to the markedly paramagnetic nature of the magnetic response of  $C_4H_4$  ( $-21$  nA/T) in  $C_8H_8$  we barely find  $-2.5$  nA/T total induced current. However, the paratropic contribution amounts to  $-8.2$  nA/T, thus we again see the rule confirmed that first and primoid second order JT distortions lead to systems with paramagnetic response. In this case however the total paramagnetic response is too weak to assign the predicate “antiaromatic” to this molecule. One reason is that the *second* second order JT distortion (which for itself is not of primoid type since the degeneracy of the frontier orbital has already been lifted to  $b_{1u}$  and  $b_{2u}$ ) causes a further increase of the HOMO-LUMO energy gap to  $9.7$  eV at HF level of theory, thus diminishing the magnetic response accordingly. For comparison the value for  $C_4H_4$  at the same level of theory (HF) is  $7.2$  eV.

### 7.3 The General $4n$ $\pi$ annulene and double bond localization (bond length alternation)

In antiaromatic  $n$ -annulenes ( $C_{4n}H_{4n}$ ) in the idealized  $D_{(4\cdot n)h}$  symmetry, double bond localisation can be easily understood as a second order (primoid) JT effect. The saddle point in these cases would have a double occupied  $e_{nu}$  or  $e_{ng}$ , for even  $n$  or for odd  $n$  orbital, respectively, thus an  $(e_{nu})^2$  or  $(e_{ng})^2$  configuration, that can distort via a  $b_{1g}$  mode to  $D_{(2\cdot n)h}$  symmetry, leading to a branching of  $e_{nu}$  to  $b_{1u}$  and  $b_{2u}$  for even  $n$  or similarly with gerade symmetry  $g$  for odd  $n$ , which would correspond in analogy to the above discussed  $C_8H_8$  to a double bond localization in the first instance.

An introductory discussion of the view of double bond localisation in ring systems as a JT distortion as well as its relation to the Perils distortion in polyethin is given in ref. <sup>15</sup>.

### 7.4 $MnF_3$

Manganese trifluoride is a prime example for a first order Jahn-Teller effect which would give in  $D_{3h}$  (a non-isometric point group) an  $E'$  ground state. In fact the lowest energy species is in the  ${}^5B_1$  electronic ground state a planar  $C_{2v}$  symmetric structure which was predicted theoretically and confirmed by gas-phase electron-diffraction <sup>16</sup>. Magnetic response calculations indeed show magnetically induced paratropic currents around the central manganese atom (see Figures 7 and 8).

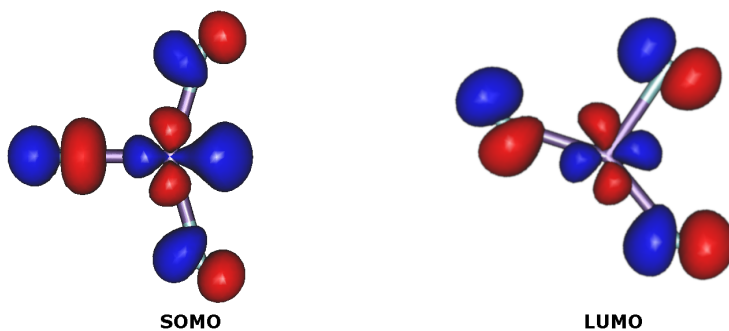


Figure 7: The  ${}^5B_1$  electronic ground state structure of  $MnF_3$  with  $C_{2v}$  symmetry and the  $b_1$  SOMO and  $a_1$  LUMO frontier orbitals including the matrix element for the virtual angular momentum transition between them. The rotational relation between the orbitals is already noticeable with bare eye.

Unlike in the previous two examples the induced paramagnetism is hidden to some extent, since experimentally the permanent magnetic moment resulting from spin dominates the magnetic properties and for the other since in this case the paramagnetic currents are atom-centered

which hampers the computational analysis of the current densities due to interference with other atomic current contributions. In addition though,  $\text{MnF}_3$  can be observed in the gas-phase<sup>16</sup>, in condensed matter a threefold coordinated  $\text{Mn}^{3+}$  cation is coordinatively highly unsaturated, thus such species will under normal conditions not be observable.

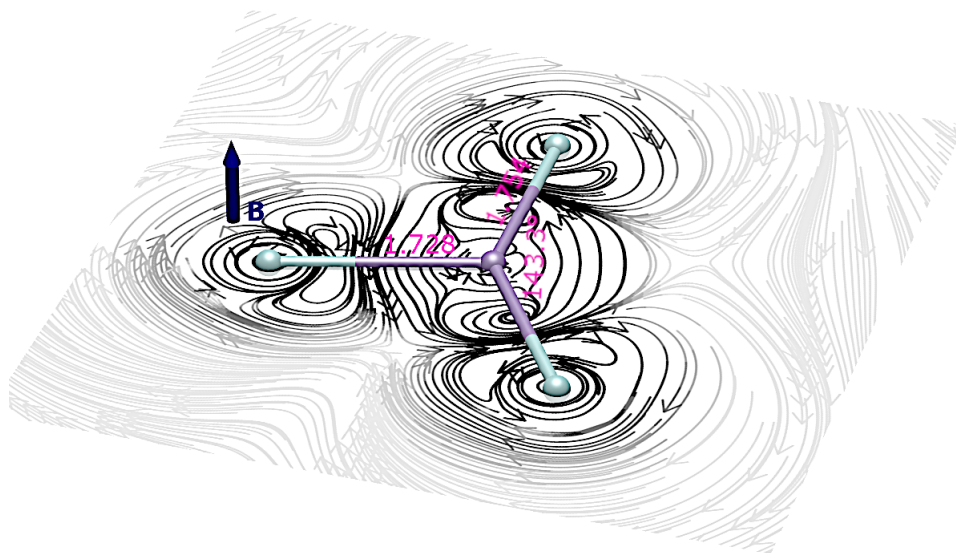
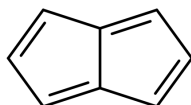


Figure 8: The  ${}^5B_1$  electronic ground state structure of  $\text{MnF}_3$  with  $C_{2v}$  symmetry and a streamline plot of the magnetically induced currents in the molecular plane ( $\mathbf{B}$  field is set perpendicular to the molecular plane). A paratropic current vortex (counterclockwise) around the Mn atom is found.

## 7.5 Pentalene

An interesting case that at first sight seems to be an outlier of our antiaromaticity symmetry rule is pentalene (see below for a molecular formula). Pentalene is a well-known case of antiaromaticity and its magnetisability was recently studied computationally<sup>17</sup>. Its apparent JT idealized symmetry would be  $D_{2h}$  (with HOMO  $a_u$  and LUMO  $b_{1u}$ ) while its computationally predicted and experimentally confirmed minimum structure is  $C_{2d}$  (HOMO:  $a_u$ , LUMO  $a_u$ ). However,  $D_{2h}$  is clearly a class  $\mathcal{K}_{aaa}$  point group, thus the observed  $D_{2h} \rightarrow C_{2d}$  distortion cannot be interpreted as a primoid second order type JT (as outlined in section 5), nevertheless we observe strong paramagnetic response that is dominated by the HOMO-LUMO virtual excitation and a distortion that is in agreement with a double-bond localisation. In essence the

decisive argument in this case is that we have to deal with a ring system containing a set of conjugated double bonds on its perimeter. Thus a natural way of interpretation would be to classify pentalene as a perturbed eight membered ring, that derives from an idealized but perturbed  $D_{8h}$  point group symmetry, with the perturbation being the additional transannular C-C bond. In this way the fact that the direct products of the HOMO-LUMO IRs are identical to the IR of  $I_z$  is mostly easily seen from the branching of  $D_{8h}$ 's  $e_{2u}$  into these HOMO,LUMO IRs.

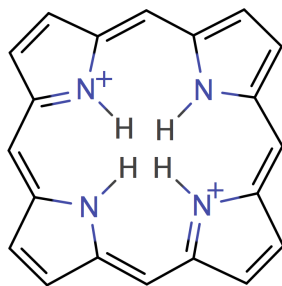


pentalene

Therefore pentalene cannot directly from its point groups ( $D_{2h}$ ,  $C_{2d}$ ) be classified as an antiaromatic compound by using our symmetry rule (though  $D_{2h}$  is not exactly low-symmetric as well).

## 7.6 Antiaromatic porphyrinoids

In analogy to the case of pentalene, a distortion out of a higher idealised symmetry can be already induced by the molecular configuration without necessitating a JT distortion. Other examples for this might be found in some porphyrinoid species, where either already the molecular configuration cannot be brought into agreement with an ideal say  $D_{4h}$  symmetry, alternatively this might be induced by coordination. A simple example would be the porphyrin-21,23-dium cation ( $H_2por^{2+}$ , see the scheme below), a derivative of which was studied for example by Štěpánek, Andrushchenko, Ruud, and Bouř<sup>18</sup>. The perturbation from an ideal  $D_{4h}$  symmetry in this case is induced by sterical strain caused by the four protons, that are closely approaching each other and cause a distortion to  $C_{2v}$  symmetry in this particular case. In the MO scheme (Fig. 7 right panel in ref<sup>18</sup>) The rotational relation between HOMO and LUMO is obvious.



porphyrin-21,23-dium cation ( $\text{H}_2\text{por}^{2+}$ )

We note that especially in such cases a double bond localization, would not necessarily have to take place, for example if by a higher than second order JT effect the lifted  $e_u$  degeneracy would lead to a stabilisation. Take a deformation of  $\text{C}_8\text{H}_8$  from  $D_{8h}$  to  $D_{2h}$  symmetry (by “squeezing” the octagon), that would yield  $e_{2u} \rightarrow a_u \oplus b_{1u}$ , which according to the JT theorem would have a zero gradient of the orbital energy with respect to the distortion (tangential branching), then it will depend on the higher order derivatives if and how large a stabilization can result from the distortion. For these considerations one should bear in mind that in principle very large values for even high order energy derivatives can occur. In such cases a double bond localisation is not necessary, while of course still paramagnetic response can be expected.

## 8 Chemical interpretation of paramagnetic response currents

Equation 2 means that a magnetic field probes the accessibility of virtual states that ideally are spatially very closely related, in only differing by the rotational orientation. In case a, possibly small, molecule responds with a strong paratropic current density this means there is a situation of close to degeneracy resembling the spatial symmetry of an atomic open subshell. The optimal symmetry/energy relation in question of eq. 2, actually can be interpreted as the analog to an atomic open subshell case for a general molecular system, and the magnetic response is a concise probe for that. In addition one also yields information on the direction of the symmetry relation from the direction of the field  $\mathbf{B}$ .

It is useful to recall that this type of degeneracy that is probed by the magnetic field is not the only possible type. Other types of (near) degeneracy include ones derived from what is sometimes called “accidental” degeneracy where there is no obvious (close-to-)symmetry relation in  $O(3)$  between occupied and empty levels and hence no contribution to paramagnetic response from these. A famous but for itself very peculiar example, since it actually goes back to the ‘hidden’  $SO(4)$  symmetry of the Coulomb potential, would be the hydrogen atomic states, *e.g.*  $2s$  and  $2p_{x,y,z}$  and for larger molecules any numerical degeneracy between levels that cannot be

traced back to symmetries in general.

Another example are degeneracies from higher than two-dimensional IRs where the rotation representation is not necessarily contained in all possible pairs of branches of IRs. This immediately casts questions on the possibility or the nature (in case one would drop the magnetic criterion) of a “3D-antiaromaticity”, a subject which must be left open in this work.

## 9 Physical interpretation and connection of induced paramagnetism and bonds

In contrast the antithetical concept of aromaticity is characterized by induced diamagnetic currents. In the common gauge origin approach, diamagnetic currents to first order are determined by the ground eigenstate  $\Psi_0$  of the  $\mathbf{B}$  field free system and correspond to a precession motion of the electrons in the magnetic field that increases the average expected angular momentum  $\langle \Psi | \hat{l}_z | \Psi \rangle$ , (for  $\Psi$  the wave function in the magnetic field) which will lead in general if the ring current extends over a sufficiently large domain covering sufficiently much of the total electron density in the molecule to an increase in total energy.

An alternative way is to describe diamagnetic response via the “Continuous Transformation of the Origin of the Current Density” (CTOCD-DZ) approach that was introduced to theoretical chemistry by Keith & Bader in 1992<sup>19</sup> that allows in particular within to Fowler & Steiner’s ipso-centric *ansatz*<sup>7</sup> to express the full magnetic response, completely in terms of occupied to virtual state (or orbital) transitions.

In this model the diamagnetic currents are determined by virtual transitions of dipole symmetry, namely dipole transition moments perpendicular to the external field  $\mathbf{B}$ . That means that for example sigma bonds that leave pairs of  $\sigma$  and  $\sigma^*$  type occupied and virtual orbitals, where the bond direction is perpendicular to the external field, contribute to the diamagnetic response. A simple example would be a bonding orbital that has some anti-bonding counterpart with a nodal plane parallel to  $\mathbf{B}$ .

In that way an electronic structure that contains covalent or systems of delocalized covalent bonds (and naturally the corresponding anti-bonding orbitals unoccupied) is diamagnetic. So we can summarize that diamagnetic response current is a consequence of (full) occupation of bonding orbitals and empty antibonding orbitals, which differ from bonding orbitals by additional nodal planes parallel to  $\mathbf{B}$ . Whereas paramagnetic response indicates incompletely occupied molecular shells which are similar up to a rotation around an axis parallel to  $\mathbf{B}$ . This in effect leads to a distinctly different picture of antiaromaticity as it was originally envisaged by Breslow as he for instance noted “Thus antiaromaticity is a particular aspect of anti-bonding, just as aromaticity is a particular aspect of bonding”<sup>3</sup>, which is according to our analyses not



the case since its not the occupation of anti-bonding orbitals that lead to the characteristic paramagnetic response currents, nor would it lead to a peculiar small HOMO-LUMO energy gap in general, or be connected with structural distortions.

Yet a more generalizing way of view is that diamagnetism indicates situations of electron delocalized bonds while paramagnetism indicates situations of incompletely filled molecular shells. And adopting a purely physical point of view, one can formulate, that proper bonds have a tendency to undergo precession motions in the same way electrons would that are orbiting in quasi-classically stable trajectories, while for symmetry reasons instable trajectories from a near-degenerate trajectory space lead to precession motions within this space but in opposite direction as compared to the diamagnetic case.

At quick glance it might be surprising that antiaromaticity has often been observed or at least proposed for organic ring systems and related species like polycyclic molecules. In contrast antiaromaticity is rarely mentioned in the context of inorganic coordination compounds and metal clusters. On the bases of our findings this is easily explained, because the vast majority of organic ring systems and related compounds can be deduced from the particular point groups  $\mathcal{K}_{ae}$ , that is non-isometric point groups with degenerate real irreducible representations. In exactly this symmetry family we have the strict relation between JT distortion and paramagnetic response. While the majority of 3D-cluster systems or coordination compounds are derived from isometric point groups where this strict correspondence does not exist. In addition coordination compounds are of course metal-centered and at least experimentally the induced paramagnetism there is often masked by permanent magnetic moments centered at the metal atoms.

The here introduced analyses might serve as a basis for a deeper understanding of antiaromaticity, but despite its principle significance, antiaromaticity is not a widely spread chemical phenomenon (for obvious reasons, since it is not only connected with structural instability but also instability in the sense of high reactivity by virtue of the small energy gap between occupied and virtual states). At this stage one might speculate if there is some consistent way to define aromaticity by the absence of paramagnetism alone, an idea going back to Bilde & Hansen<sup>20</sup>. In that way the presence or absence of rotationally accessible virtual states and their intimate connection with structural distortions could eventually be the only decisive criteria for presence or absence of aromaticity or antiaromaticity.

## 10 A “numeric” version of the principle and implications for a possible rule for antiaromaticity

The symmetry connection between rotational virtual excitations and the Jahn-Teller effect in a subfamily of the point groups deepens our understanding of antiaromaticity. On the one hand, this connection, however cannot be established in the general case of an antiaromatic molecule by pure symmetry considerations, not even in the case of a relatively high symmetry like pentalene. This is the usual restriction underlying any symmetry selection rule (take diople transitions for electronic excitations by light). An open question in this context also is if there is a deeper connection between the numerator and the denominator in expression 3, which intuition might suggest: two orbitals that are very similar in shape and only differ by orientation necessarily should have similar energies. An open question is: In how far can we expect the opposite as well?

On the other hand the bare symmetry rule or numerical principle (*i.e.* the conditions under which to observe large terms 3) again cannot provide us with a precise condition as to when a specific case is to be considered antiaromatic and when not. We even notice a paradoxical component: the stronger the distortion the smaller the terms in expression 3 are getting (by both an increase in the denominator and a decrease in the numerator) and the weaker the paramagnetic response will be in general. Also a strong paramagnetic response shall make one expect a low degree of distortion as well. In that sense we rather expect that all systems that meet the IUPAC definition (that without a doubt by construction is based on observed real world examples) are those that find a kind of balance between the extremes of distortion and paramagnetism.  $C_8H_8$  misses it due to the strong distortion while there might be other cases of strong paramagnetism that show less or no distortion contrary to expectation. Take for example a transition state of a  $2 + 2$  cycloaddition reaction.

Thus the concept of antiaromaticity appears as a principle of instability, (even with respect to its own definition integrity). Nevertheless its a concept that can be sensitively verified (or falsified) both in the real world and in the computer by energetic, structural and magnetic methods.

An extension of these considerations we are currently working on is the analysis of the symmetry rules of magnetic response and JT distortion in the fully relativistic domain including spin-orbit coupling.

## 11 Conclusion

We have shown by symmetry considerations how Jahn-Teller distortion and paramagnetic response are intimately related in the family of points groups comprised of  $C_n$ ,  $C_{nv}$ ,  $C_{nh}$ ,  $D_n$ ,  $D_{nd}$ ,  $D_{nh}$ ,  $S_{2n}$  for  $n > 2$ . We suggest that this connection is the underlying symmetry principle of antiaromaticity, since the latter is defined by the central properties of a small HOMO-LUMO

gap, proneness to structural distortion or instability and magnetically induced paramagnetic ring currents. We also saw that electronic structure related to covalent or delocalized covalent bonding or filled atomic subshells followed by empty subshells is related to diamagnetic response while electronic situations resembling open atomic subshells are related to paramagnetic response. The sparsity of examples may not only go back to the fact that antiaromaticity is related to low energetic stability but also due the paradoxity between distortion and paramagnetism that is hidden under its definition and that we have revealed in this work.

## References

- [1] Solà, M. Connecting and combining rules of aromaticity. Towards a unified theory of aromaticity. *WIREs, Comp. Mol. Sci.* (2018).
- [2] Janda, T. & Foroutan-Nejad, C. Why is benzene unique? Screening magnetic properties of C<sub>6</sub>H<sub>6</sub> isomers. *Chem. Phys. Chem.* **19**, 2357–2363 (2018).
- [3] Breslow, R. Antiaromaticity. *Acc. Chem. Res.* **6**, 393–398 (1973).
- [4] International Union of Pure and Applied Chemistry, IUPAC Compendium of Chemical Terminology – The Gold Book (2006).
- [5] Minkin, V. I. Glossary of terms used in theoretical organic chemistry — Pure and Applied Chemistry. *Pure Appl. Chem.* **71**, 1919 – 1981 (2009).
- [6] Lazzeretti, P. Ring currents. *Prog. Nuc. Mag. Res. Spec.* **36**, 1 – 88 (2000).
- [7] Steiner, E. & Fowler, P. W. Four- and two-electron rules for diatropic and paratropic ring currents in monocyclic systems. *Chem. Commun.* 2220–2221 (2001).
- [8] Sulzer, D., Olejniczak, M., Bast, R. & Saue, T. 4-component relativistic magnetically induced current density using London atomic orbitals. *Phys. Chem. Chem. Phys.* **13**, 20682–20689 (2011).
- [9] Bersuker, I. B. Recent developments in the Jahn–Teller effect theory. In Köppel, H., Yarkony, D. & Barentzen, H. (eds.) *The Jahn-Teller Effect*, vol. 97 of *Springer Series in Chemical Physics*, chap. 1, 3–23 (Springer, Berlin, Heidelberg, 2009), 1 edn.
- [10] Albright, T. A., Burdett, J. K. & Whangbo, M. *Orbital Interactions in Chemistry*, chap. 7, 134–136 (John Wiley & Sons, Inc., Hoboken, New Jersey, 2013), 2 edn.
- [11] Liu, Y., Wang, Y. & Bersuker, I. B. Geometry, electronic structure, and pseudo Jahn-Teller effect in tetrasilacyclobutadiene analogues. *Sci. Rep.* **6**, 23315 EP (2016).

- [12] Nakamura, K., Osamura, Y. & Iwata, S. Second-order Jahn-Teller effect of cyclobutadiene in low-lying states. An MCSCF study. *Chem. Phys.* **136**, 67 – 77 (1989).
- [13] Jusélius, J. & Sundholm, D. The aromaticity and antiaromaticity of dehydroannulenes. *Phys. Chem. Chem. Phys.* **3**, 2433–2437 (2001).
- [14] Karadakov, P. B. Aromaticity and antiaromaticity in the low-lying electronic states of cyclooctatetraene. *J. Phys. Chem. A* **112**, 12707–12713 (2008).
- [15] Hoffmann, R. *Solids and Surfaces: A Chemist's View of Bonding in Extended Structures* (Wiley-VCH, New York, 1989), 1 edn.
- [16] Hargittai, M., Réffy, B., Kolonits, M., Marsden, C. J. & Heully, J.-L. The structure of the free MnF<sub>3</sub> molecule — a beautiful example of the JahnTeller effect. *J. Am. Chem. Soc.* **119**, 9042–9048 (1997).
- [17] Sundholm, D., Berger, R. J. F. & Fliegl, H. Analysis of the magnetically induced current density of molecules consisting of annelated aromatic and antiaromatic hydrocarbon rings. *Phys. Chem. Chem. Phys.* **18**, 15934–15942 (2016).
- [18] Štěpánek, P., Andrushchenko, V., Ruud, K. & Bouř, P. Porphyrin protonation studied by magnetic circular dichroism. *J. Phys. Chem. A* **116**, 778–783 (2012).
- [19] Keith, T. A. & Bader, R. F. Calculation of magnetic response properties using a continuous set of gauge transformations. *Chem. Phys. Lett.* **210**, 223 – 231 (1993).
- [20] Bilde, M. & Hansen, A. E. Ab initio study of the Pauling-London-Pople (ring current) effect: LORG calculation and analysis of the NMR shielding tensors in a Sondheimer aromatic annulene and a non-aromatic analogue. *Mol. Phys.* **92**, 237–250 (1997).
- [21] Schmidt, M. W. *et al.* General atomic and molecular electronic structure system. *J. Comp. Chem.* **14**, 1347–1363.
- [22] Voter, A. F. & Goddard, W. A. The generalized resonating valence bond description of cyclobutadiene. *J. Am. Chem. Soc.* **108**, 2830–2837 (1986).
- [23] Schäfer, A., Horn, H. & Ahlrichs, R. Fully optimized contracted Gaussian basis sets for atoms Li to Kr. *J. Chem. Phys.* **97**, 2571–2577 (1992).
- [24] Allouche, A.-R. Gabedit – A graphical user interface for computational chemistry softwares. *J. Comp. Chem.* **32**, 174–182.
- [25] ReSpect 4.0.0 (2016), relativistic spectroscopy DFT program of authors M. Repisky, S. Komorovsky, V. G. Malkin, O. L. Malkina, M. Kaupp, K. Ruud, with contributions from R. Bast, R. Di Remigio, U. Ekstrom, M. Kadec, S. Knecht, L. Konecny, E. Malkin, I. Malkin Ondik (see <http://www.respectprogram.org>).

- [26] Dyll, K. G. Relativistic double-zeta, triple-zeta, and quadruple-zeta basis sets for the 4s, 5s, 6s, and 7s elements. *J. Phys. Chem. A* **113**, 12638–12644 (2009).
- [27] Persistence of Vision Pty. Ltd. (2004) Persistence of Vision Raytracer ( Version 3.6) [Computer software], Retrieved from <http://www.povray.org/download/>.
- [28] Perdew, J. P., Ernzerhof, M. & Burke, K. Rationale for mixing exact exchange with density functional approximations. *J. Chem. Phys.* **105**, 9982–9985 (1996).

## 12 Acknowledgments

The work has been performed under the Project HPC-EUROPA3 (INFRAIA-2016-1-730897), with the support of the EC Research Innovation Action under the H2020 Programme; in particular, RB gratefully acknowledges the support of Prof. Dr. Dage Sundholm from the University of Helsinki and the computer resources and technical support provided by the CSC Helsinki. RB also acknowledges Prof. Dr. Dage Sundholm for financial support and Prof. Dr. Martin Breza from the Slovak University of Technology (Bratislava), Prof. Dr. Paolo Lazzeretti (Modena) and Prof. Dr. Juha Vaara (Oulu) for fruitful discussions and Prof. Dr. Nicola Hüsing (Salzburg) for generous and kind support of all research activities.



# A Supporting Information

## A.1 Character tables

Table 1:  $Alt^2$  tables for all point groups

(a)  $\mathcal{K}_{aaa}$  point groups

p.grp	$C_1$	$C_s$	$C_2$	$C_i$	$C_{2v}$	$C_{2h}$	$D_2$	$D_{2h}$
$\Gamma_{l_z}$	$A$	$A'$	$A$	$A$	$A_2$	$A_g$	$B_1$	$B_{1g}$

(b)  $\mathcal{K}_{ae}$  cyclic-based point groups

p.grp, $n \geq 1$	$C_{2n+1}$	$C_{2n+2}$	$C_{(2n+1)v}$	$C_{(2n+2)v}$	$C_{(2n+1)h}$	$C_{(2n+2)h}$	$S_{4n}^{(*)}$	$S_{4n+2}$
$\Gamma_e, i = 1 \dots n$	$E_i$	$E_i$	$E_i$	$E_i$	$E'_i, E''_i$	$E_{ig}, E_{iu}$	$E_i$	$E_{ig}, E_{iu}$
$Alt^2(\Gamma_e)$	$A$		$A_2$		$A'$	$A_g$	$A$	$A_g$

(\*) :  $i$  ranges from 1 to  $2n - 1$

(c)  $\mathcal{K}_{ae}$  dihedral-based point groups

p.grp, $n \geq 1$	$D_{2n+1}$	$D_{2n+2}$	$D_{(2n)d}^{(*)}$	$D_{(2n+1)d}$	$D_{(2n+1)h}$	$D_{(2n+2)h}$
$\Gamma_e, i = 1 \dots n$	$E_i$	$E_i$	$E_i$	$E_{ig}, E_{iu}$	$E'_i, E''_i$	$E_{ig}, E_{iu}$
$Alt^2(\Gamma_e)$	$A_2$		$A_2$	$A_{2g}$	$A'_2$	$A_{2g}$

(\*) :  $i$  ranges from 1 to  $2n - 1$

(d)  $\mathcal{K}_t$  type cubic point groups

p.grp	$T$		$T_d = O$			$T_h$				$O_h$					
$\Gamma_l$	$T$		$T_1$			$T_g$				$T_{1g}$					
$\Gamma$	$E$	$T$	$E$	$T_1$	$T_2$	$E_g$	$T_g$	$E_u$	$T_u$	$E_g$	$T_{1g}$	$T_{2g}$	$E_u$	$T_{1u}$	$T_{2u}$
$Alt^2(\Gamma)$	$A$	$T$	$A_2$	$T_1$	$T_1$	$A_g$	$T_g$	$A_g$	$T_g$	$A_{2g}$	$T_{1g}$	$T_{1g}$	$A_{2g}$	$T_{1g}$	$T_{1g}$

(e)  $\mathcal{K}_t$  type icosahedral groups

p.grp	$I$				
$\Gamma_l$	$T_1$				
$\Gamma$	$T_1$	$T_2$	$G$		$H$
$Alt^2(\Gamma)$	$T_1$	$T_2$	$T_1 \oplus T_2$		$T_1 \oplus T_2 \oplus G$

p.grp	$I_h$							
$\Gamma_l$	$T_{1g}$							
$\Gamma$	$T_{1g}$	$T_{2g}$	$G_g$		$H_g$		$T_{1u}$	$T_{2u}$
$Alt^2(\Gamma)$	$T_{1g}$	$T_{2g}$	$T_{1g} \oplus T_{2g}$		$T_{1g} \oplus T_{2g} \oplus G_g$		$T_{1g}$	$T_{2g}$

## A.2 Computational details

### A.2.1 C<sub>4</sub>H<sub>4</sub>

The geometry optimization of 1,3-cyclobutadiene in  $D_{4h}$  symmetry was performed with the GAMESS-US<sup>21</sup> programme package (version 5DEC 2014 (R1)) for a reason lined out below and in the spirit of an early work from Voter and Goddard at the generalized valence bond - perfect pairing (GVB(PP)) level of theory<sup>22</sup> and using the Karlsruhe def-TZVPP basis sets for carbon and hydrogen<sup>23</sup>. Starting orbitals and geometry were used from a restricted Hartree-Fock (RHF) calculation for the dianionic species [C<sub>4</sub>H<sub>4</sub>]<sup>2-</sup>, restricted to  $D_{4h}$  spatial symmetry (but the wave function is effectively treated in GAMESS as  $D_{2h}$  since no higher wave function symmetries are available in the current versions of GAMESS-US). For the subsequential GVB run 13 doubly occupied inactive orbitals and 1 electron pair in 2 orbitals were set. That setting completely is equivalent to a complete active space two electrons in two orbitals computation (CAS(2i2)). We note that convergence of GVB in cases can be considerably slower and in cases of problems with the starting orbitals it seems convenient to converge the orbitals in an actual CAS(2i2) run, that for example can be run using the full-Newton-Raphson converger that is implemented in GAMESS-US. The main reason for choosing GVB(PP) instead of CAS was to be able to extract orbital energies from a “multiconfigurational” wave function, in order to demonstrate the branching and energy changes of the orbitals, that is essential for the *primoid* second order Jahn-Teller cases.

The optimization resulted in the following structure and energy:

---

C4H4.D4h_eq.GVB-PP_TZVPP.txt				
<hr/>				
C4H4, D4h, GVB(PP)/def-TZVPP, units of    and hartree				
E=	-153.6925014955	GRAD. MAX=	0.0000280	R.M.S.= 0.0000162
C	6.0	-0.7131801506	-0.7131801826	-0.0000000000
C	6.0	0.7131801506	-0.7131801826	0.0000000000
C	6.0	-0.7131801506	0.7131801826	0.0000000000
C	6.0	0.7131801506	0.7131801826	0.0000000000
H	1.0	-1.4687380037	-1.4687382006	-0.0000000000
H	1.0	1.4687380037	-1.4687382006	0.0000000000
H	1.0	-1.4687380037	1.4687382006	0.0000000000
H	1.0	1.4687380037	1.4687382006	0.0000000000

---

The  $D_{2h}$  minimum was calculated by choosing  $D_{2h}$  symmetry in the input and slightly distorting the coordinates to some off- $x$ ,  $y$ -diagonal value but using the starting orbitals from the  $D_{4h}$  run. The optimization resulted in the following structure and energy:

---

C4H4.D2h_eq.GVB-PP_TZVPP.txt				
------------------------------	--	--	--	--

---



C4H4, D2h, GVB(PP)/def-TZVPP, units of and hartree

E= -153.7126953359 GRAD. MAX= 0.0000191 R.M.S.= 0.0000099

C	6.0	-0.7761786150	-0.6619033512	0.0000000000
C	6.0	0.7761786150	-0.6619033512	-0.0000000000
C	6.0	-0.7761786150	0.6619033512	-0.0000000000
C	6.0	0.7761786150	0.6619033512	-0.0000000000
H	1.0	-1.5315443480	-1.4196296797	0.0000000000
H	1.0	1.5315443480	-1.4196296797	-0.0000000000
H	1.0	-1.5315443480	1.4196296797	-0.0000000000
H	1.0	1.5315443480	1.4196296797	-0.0000000000

By a linear interpolation between the  $D_{4h}$  saddle point and the  $D_{2h}$  minimum structure 9 intermediate structures were generated and the frontier orbital energies were extracted a generate a branching plot (see Fig. 10), a schematic version of which is represented in Fig. 1 in the main text.

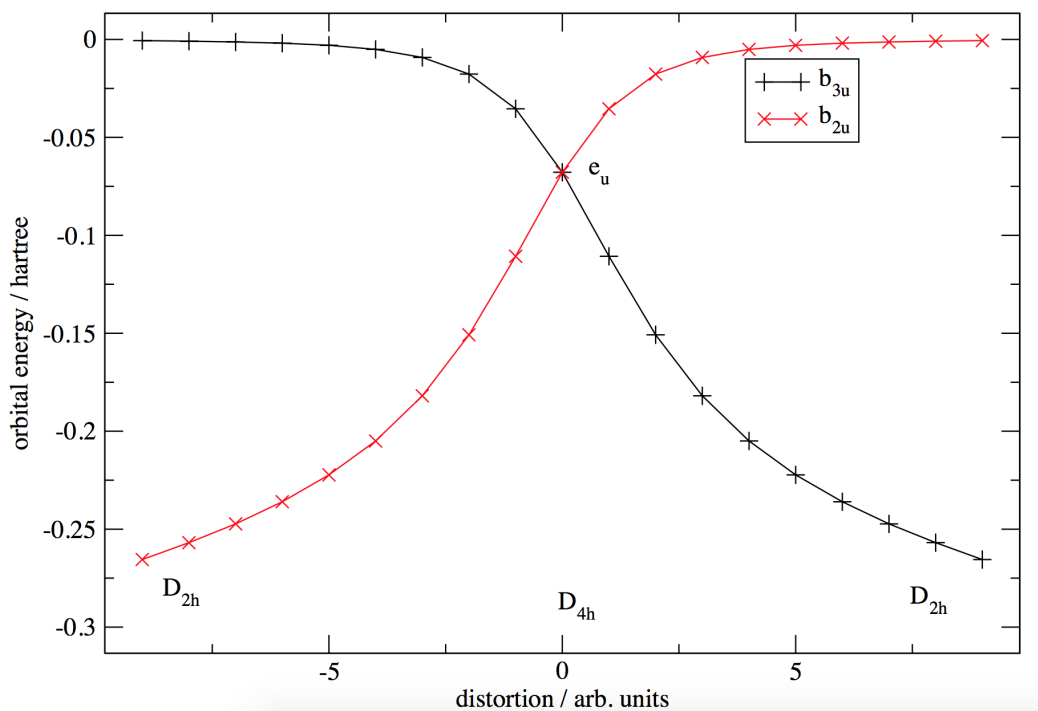


Figure 9: Frontier orbital branching in  $C_4H_4$  upon relaxed distortion from  $D_{4h}$  to  $D_{2h}$  at GVB(PP)/def-TZVPP level of theory.

The corresponding state energies of first two singlet states ( $1^1A_g$  and  $2^1A_g$ ) have been com-

puted for the intermediate structures complemented by two more strongly distorted structures by the analogous CAS(2i2) state average calculation. In this way one can see a representation of the JT-coupling between the two states (see Fig. 9).

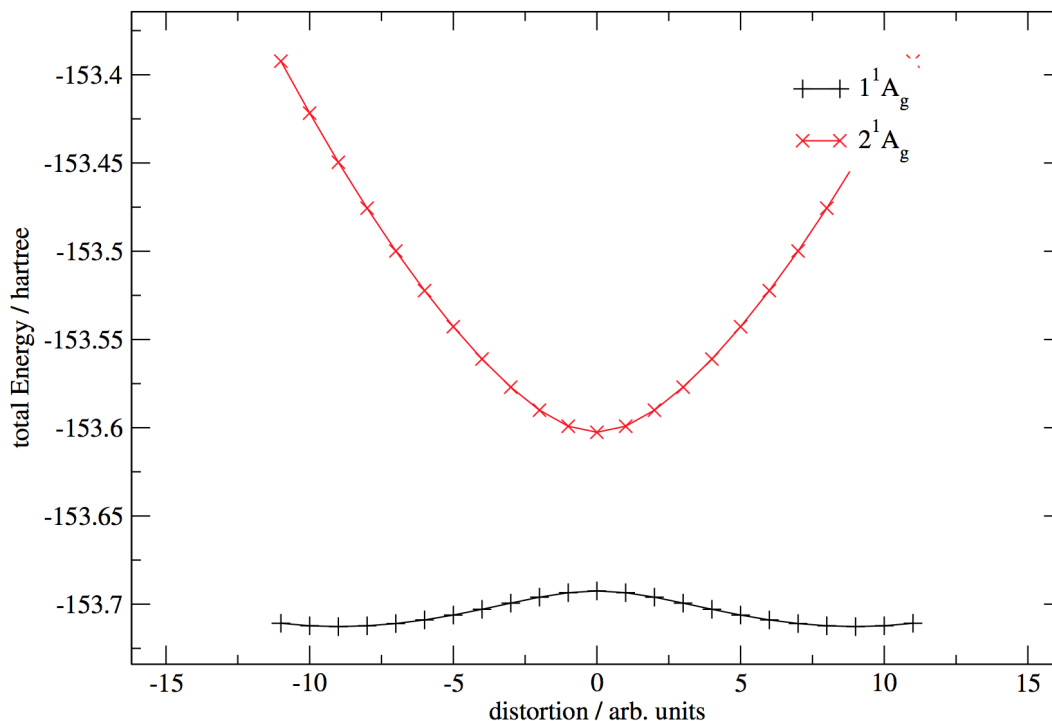


Figure 10: Lowest two singlet states in  $C_4H_4$  upon relaxed distortion from  $D_{4h}$  to  $D_{2h}$  at state average CAS(2i2i)/def-TZVPP level of theory

The orbital plots in Figures 5, 5 and 7 were generated with the program gabedit<sup>24</sup>.

Magnetically induced currents were calculated for the  $D_{2h}$  minimum structure using the program ReSpect (version 4.0.0) from Repisky and Komorovsky<sup>25</sup>. Since for the  $D_{2h}$  minimum structure the CI coefficients of the two configurations from the GVB(PP) calculation were only 0.980137, and -0.198321 respectively (corresponding to a weight of only about 4% of the second configuration), a single reference method can be used safely for computation of the magnetic response. To stay consistent we have also used for the magnetic response the HF level of theory and the Dyalls (relativistic) triple- $\zeta$  basis sets for C and H<sup>26</sup>.

For the wave function calculation the GVB(PP) structure has been used a point nucleus model, the “mdhf” method (multicomponent Dirac-HF hamiltonian) but quasi-non relativistic settings “cscale=20.0” and “soscale=0.0” and “grid: large”.

The magnetic response calculation was done using the London orbital approach (GIAO) and the ‘dft-kernel: xalda’ option and the magnetic field was set perpendicular to the molecular plane.

The integration grid for the total current calculation was set to start -4 Å below the molecular

plane pass the centre of the molecule and have a width and heights of 8 Å, respectively and using  $200 \times 200$  grid points. The net currents passing that plane are calculated to 2.6748885 nA/T (diatropic) and -25.132882 nA/T (paratropic) yielding a total paratropic current of -22.457993 nA/T.

The streamline plot from Fig. 3 were generated similarly just using a current plane starting at  $x = -2.5$  and  $y = -2.5$  Å. The length and width was set to 5 Å. The streamline plot was generated using the “make-stream” script that is distributed with ReSpect. Fig. 3 was generated with Povray<sup>27</sup>.

### A.2.2 C<sub>8</sub>H<sub>8</sub>

Similar as C<sub>4</sub>H<sub>4</sub> also C<sub>8</sub>H<sub>8</sub> in full  $D_{8h}$  symmetry is a multireference case of two electrons in the doubly degenerate  $e_{2u}$  orbitals<sup>14</sup>, that has to be treated at least with a two-configuration wave function. For consistency we have applied here as well the GVB(PP)/TZVPP method with completely analogous strategy as in the case of C<sub>4</sub>H<sub>4</sub>, that is first optimization of the dianion using RHF and then followed by the symmetry restricted geometry optimization in  $D_{8h}$  with GVB using 27 doubly occupied orbitals and two orbitals with two electrons in perfect pairing to yield a second order saddle point structure (with two equally weighted configurations):

---

C8H8\_D8h\_eq.GVB-PP\_TZVPP.txt

---

C8H8, D8h, GVB(PP)/def-TZVPP, units of    and hartree

E=-307.5867677504

C	1.6802926394	0.0000000000	0.6960000000
C	-1.6802926394	0.0000000000	0.6960000000
C	1.6802926394	0.0000000000	-0.6960000000
C	-1.6802926394	0.0000000000	-0.6960000000
C	-0.6960000000	0.0000000000	-1.6802926394
C	0.6960000000	0.0000000000	1.6802926394
C	-0.6960000000	0.0000000000	1.6802926394
C	0.6960000000	0.0000000000	-1.6802926394
H	2.6743870164	0.0000000000	1.1077673732
H	-2.6743870164	0.0000000000	1.1077673732
H	2.6743870164	0.0000000000	-1.1077673732
H	-2.6743870164	0.0000000000	-1.1077673732
H	1.1077673732	0.0000000000	2.6743870164
H	-1.1077673732	0.0000000000	2.6743870164
H	1.1077673732	0.0000000000	-2.6743870164
H	-1.1077673732	0.0000000000	-2.6743870164

---

The C-C distance is 1.392 and H-H is 1.076 Å, respectively, the energy of the HOMO  $\varepsilon(e_{2u}) = -0.0608$  Hartree.

Subsequent optimization in  $D_{4h}$  results in a first order saddle point, with already a small coefficient of the second configuration ( $c_1 = 0.995999$ ,  $c_2 = -0.089369$ ) and HOMO and LUMO energies of  $\varepsilon(b_{3u}) = -0.2699$  and  $\varepsilon(b_{2u}) = 0.0000$  Hartree, the C-C distances split into two sets of 1.324 and 1.473 Å and C-H distances of 1.075 Å:

---

C8H8\_D4h\_eq.GVB-PP\_TZVPP.txt

---

C8H8, D4h, GVB(PP)/def-TZVPP, units of and hartree

E=-307.6196129777

C	1.6689419240	-0.0000000000	0.7365511863
C	1.6689419240	-0.0000000000	-0.7365511863
C	-1.6689419240	-0.0000000000	0.7365511863
C	-1.6689419240	-0.0000000000	-0.7365511863
C	0.7382750555	0.0000000000	1.6782476200
C	0.7382750555	0.0000000000	-1.6782476200
C	-0.7382750555	0.0000000000	1.6782476200
C	-0.7382750555	0.0000000000	-1.6782476200
H	2.6649503331	0.0000000000	1.1423860279
H	2.6649503331	0.0000000000	-1.1423860279
H	-2.6649503331	0.0000000000	1.1423860279
H	-2.6649503331	0.0000000000	-1.1423860279
H	1.1298611754	0.0000000000	2.6795220078
H	1.1298611754	0.0000000000	-2.6795220078
H	-1.1298611754	0.0000000000	2.6795220078
H	-1.1298611754	0.0000000000	-2.6795220078

---

Releasing the symmetry to  $D_{2d}$  yields the minimum structure, with again smaller CI coefficient for the second configuration ( $c_1 = 0.999143$ ,  $c_2 = -0.041393$ ) and HOMO and

LUMO energies of  $\varepsilon(a_1) = -0.3578$  and  $\varepsilon(a_2) = 0.0000$  Hartree; geometric parameters are  $C-C_{short/long} = 1.320/1.475 \text{ \AA}$ ,  $C-H = 1.077 \text{ \AA}$ ,  $\angle(CCC) = 127.3^\circ$ ,  $\angle^{dih}(CCCC) = 0.0/54.1^\circ$ .

---

C8H8.D2d\_eq.GVB-PP-TZVPP.txt

---

C8H8, D2d, GVB(PP)/def-TZVPP, units of and hartree

E=-307.6408330022

C	-1.5659424	0.6328078	0.3790173
C	1.5659424	0.6328078	-0.3790173
C	-1.5659424	-0.6328078	-0.3790173
C	1.5659424	-0.6328078	0.3790173
C	-0.6328078	1.5659424	0.3790173
C	0.6328078	-1.5659424	0.3790173
C	-0.6328078	-1.5659424	-0.3790173
C	0.6328078	1.5659424	-0.3790173
H	-2.4628900	0.8232252	0.9441068
H	2.4628900	-0.8232252	0.9441068
H	-2.4628900	-0.8232252	-0.9441068
H	2.4628900	0.8232252	-0.9441068
H	0.8232252	-2.4628900	0.9441068
H	-0.8232252	2.4628900	0.9441068
H	0.8232252	2.4628900	-0.9441068
H	-0.8232252	-2.4628900	-0.9441068

---

The magnetically induced currents for the  $D_{2d}$  minimum structure were calculated with the very same procedures as in case of  $C_4H_4$  and the magnetic field was set perpendicular to the average molecular plane. The integration grid for the total current calculation was set to start  $-5 \text{ \AA}$  below the molecular plane pass the centre of the molecule and have a width and heights of  $10 \text{ \AA}$ , respectively  $300 \times 300$  grid points. The net currents passing that plane are calculated to  $5.7644395 \text{ nA/T}$  (diatropic) and  $-8.2361711 \text{ nA/T}$  (paratropic) yielding a total paratropic current of  $-2.4717316 \text{ nA/T}$ . The streamline plot from Fig. 3 were generated similarly just using a current plane starting at  $x = 6$  and  $y = -6 \text{ \AA}$ . The length and width was set to  $12 \text{ \AA}$ .

### A.2.3 $MnF_3$

For the calculation of the magnetically induced molecular currents in  $MnF_3$ , we have used the experimental gas-phase structure, that is  $C_{2v}$  symmetric and corresponds to the minimum of the  $^5B_1$  electronic state<sup>16</sup> ( $Mn-F1 = 1.728 \text{ \AA}$ ,  $Mn-F2 = 1.754 \text{ \AA}$ ,  $Mn-F3 = 1.754 \text{ \AA}$  and  $\angle(F2-Mn-F3) = 143.3^\circ$ ). We have used the PBE0 hybrid density functional<sup>28</sup> as it is implemented in ReSpect (“method : mdks/pbe0”), the non-relativistic settings as described above, “multiplicity : 5” and again the relativistic basis sets from Dyall for Mn and F atoms<sup>26</sup>. In the magnetic

response calculation the DFT kernel option “xalda” was chosen. The grid plane for the current vectors was set to the  $z = 0$  plane extending 8 Å in  $x$  and  $y$  direction respectively with a grid of  $50 \times 50$  points. Otherwise the same procedure was applied as in case of  $C_4H_4$  and  $C_8H_8$ .

### A.3 Definition of Antiaromaticity

The definition of antiaromaticity which made it into the IUPACs “Gold-Book” was originally provided by V. I. Mishkin in his article about “Glossary of terms used in theoretical organic chemistry”<sup>5</sup>. The complete quote is “antiaromaticity (antithetical to aromaticity)

Those cyclic molecules for which cyclic electron delocalization provides for the reduction (in some cases, loss) of thermodynamic stability compared to acyclic structural analogues are classified as antiaromatic species. In contrast to aromatic compounds, antiaromatic ones are prone to reactions causing changes in their structural type, and display tendency to alternation of bond lengths and fluxional behavior (see fluxional molecules) both in solution and in the solid. Antiaromatic molecules possess negative (or very low positive) values of resonance energy and a small energy gap between their highest occupied and lowest unoccupied molecular orbitals. In antiaromatic molecules, an external magnetic field induces a paramagnetic electron current. Whereas benzene represents the prototypical aromatic compound, cyclobuta-1,3-diene exemplifies the compound with most clearly defined antiaromatic properties.”